MET.O.14

METEOROLOGICAL OFFICE
BOUNDARY LAYER RESEARCH BRANCH
TURBULENCE & DIFFUSION NOTE

T.D.N. No. 105

ON THE NET FORCES PRODUCED BY SURFACE MOUNTED OBSTACLES

by

P.J.Mason & R.I.Sykes

July 1978

FH18

To appear QJRMS Oct 79

On the net forces produced by surface mounted obstacles

by

P. J. Mason and R. I. Sykes

Meteorological Office Bracknell

Abstract

Numerical calculations of the forces involved in Ekman layer flow past three-dimensional topography are presented. The forces are obtained from finite-difference solutions of the Navier-Stokes equations. The results confirm expectations from earlier two-dimensional work that many flows produce no significant change in total momentum transfer between the fluid and the surface. Only flows generating some form of trailing vortex system appear capable of changing the total force on the lower boundary. The effects of Ekman boundary layer instabilities, and their interaction with topography are also discussed.

1. Introduction

An understanding of the influence of small scale topography on the atmosphere and the parametrisation of these effects in large scale models centres on the net changes in momentum transfer. In a previous paper (Mason and Sykes 1978a) we gave a general review of the magnitude of changes arising from different scales, but concentrated on larger scales for which the Rossby number was of order unity. In a more recent paper (Mason and Sykes 1979a referred to hereafter as M & S) we studied smaller scale two-dimensional flows for which separation occurred. The present paper extends the latter work to three-dimensional flows. As in M & S we deliberately choose not to include any form of turbulence modelling. Turbulence modelling in such strongly disturbed flows is at present an uncertain art without even sound empirical support. It would thus be rash to proceed with turbulence modelling until we have a reasonable understanding of the corresponding laminar flows. By laminar flow we mean a solution of the Navier-Stokes equations with a constant viscosity equal to a typical value of turbulent eddy viscosity. This means that the order of the viscous term in the Navier-Stokes equations will be the same as that of the divergence of the Reynolds stresses in the corresponding turbulent flow problem.

The basic parameter determining the character of homogeneous laminar flow is the Reynolds number $R = \bar{u}h/\nu$ where $\bar{u}$ is a typical flow speed, h a typical scale and ν the kinematic viscosity. For atmospheric flows the Reynolds number based on molecular viscosity is very large but we may ask the magnitude of a Reynolds number based on an eddy viscosity. This is a dangerous procedure because of the essential differences between laminar and turbulent flows.

However, remembering this qualification, some order of magnitude calculations seem worthwhile. If we consider an object in the approximately logarithmic part of the turbulent boundary layer (say less than 50 m height) then we may define a Reynolds number

$$R_T = \bar{u}h/\nu_T$$

In this region the eddy viscosity $\nu_T \simeq k u_* Z$ where k is the von Karman constant, u_* the friction velocity and Z distance from the boundary. Thus taking $Z \simeq h$ we have

$$R_T \simeq \frac{\bar{U}}{k u_*} .$$

Now $u_*^2 = c_D U_g^2$ where c_D is the so-called geostrophic drag coefficient and U_g the geostrophic wind. Taking $\bar{U} \simeq U_g$ we have

$$R_T \simeq \frac{1}{k c_D^{\frac{1}{2}}}$$

Hence with $k = 0.4$ and $c_D = 2.10^{-3}$ we have typically

$$R_T \simeq 60.$$

For obstacles larger than the logarithmic region but still immersed in the boundary layer a reasonable estimate of ν_T is given by considering the implied surface stress

$$\text{i.e.} \quad \frac{U_g \nu_T}{\delta} = c_D U_g^2$$

where δ is the depth of the boundary layer. Thus

$$\nu_T = c_D \delta U_g$$

and taking $\delta = 10^3$ m and $c_D = 2.10^{-3}$ as typical, we obtain

$$R_T \simeq \frac{h}{2} \qquad (\text{with } h \text{ in metres}).$$

In what precedes we have assumed the vertical scale of the topography to be comparable with the horizontal but for relatively larger horizontal scales a different Reynolds number may be associated with horizontal motions. This was discussed in M & S but for completeness we note here that the observed horizontal Reynolds stress components are always comparable with the vertical, ie in terms of eddy viscosity

$$\nu_{TH} \frac{U_g}{L} \simeq \nu_T \frac{U_g}{\delta}$$

where ν_{TH} is the horizontal eddy viscosity and L the horizontal scale. Thus

$$R_{TH} = \frac{U_g L}{\nu_{TH}} = \frac{\delta}{2} \qquad \text{(with } \delta \text{ in metres)}.$$

It is important that these rough calculations should not be taken as more than order of magnitude estimates, but they serve to indicate ranges of Reynolds numbers of relevance to the atmospheric dynamics.

In M & S, two-dimensional integrations of the Navier-Stokes equations were made in this general range of Reynolds numbers. One of the main results was the observation that for steady homogeneous flows, even when separation occurred, the topography produced little net change in total drag. The pressure force on the topography was nearly balanced by a reduction in viscous surface stress. This result and the details of these flows were shown to be well predicted by 'triple deck' boundary layer theory (Sykes 1978). This theory also predicts a similar small net change in total drag for three-dimensional flows (Sykes 1979). Although the agreement with the Navier-Stokes equations was shown to be good with $Re = U_g \delta/\nu = 600$, the theory is strictly only valid in the limit of large Reynolds number.

No analytic solution is available for moderate Reynolds numbers but for small Reynolds numbers ($<< 1$) we can turn to existing work. Wang (1978) considers slow flow over a corrugated base in a channel with a rigid upper surface. An expression for the net force is given and in the limit, as the depth of the channel is much larger than the height of the corrugations, the net effect is zero. Thus with analytic support for steady flow at large and small Reynolds numbers the results obtained for steady flows at moderate Reynolds numbers are perhaps to be expected.

The two-dimensional homogeneous flows did not always give zero net drag on these small length scales. When the flow was unsteady, with eddies being generated, important net drags occurred. The eddies were shed by topography at Reynolds numbers above a value depending on the slope (eg $R \simeq 30$ for slope $\sim 1/5$; $R \simeq 500$ for slope $\sim 1/10$). In a narrow range of parameters a smaller but significant increase in drag occurred when unsteady eddies appeared downstream of the topography. These had scale less than the topography and a character similar to Ekman roll instabilities. The orientation of our two-dimensional domain (parallel to the geostrophic flow) does not favour such instabilities and it was felt important to investigate this effect in three-dimensional motion.

In the present three-dimensional study a number of significant results have emerged. As expected from the analytical considerations most steady separated flows gave no significant net drag. A significant net drag was found only when there was evidence for the generation of trailing vortices by the topography. This generally became important before but close to the parameters for which the flow also became unsteady ($R \gtrsim 100$ for a slope of unity). When the basic flow was unstable to Ekman rolls the only effect of topography appeared to be on the phase of the rolls; keeping them nearly stationary in the lee. In our only integration with a stable boundary layer no topographically induced rolls were observed.

The details of the force results and further interpretation are given in § 3. In § 2 we outline the numerical model used in this study and in §4 we present the conclusions. The violent three-dimensional flows considered in this paper have not been realised in previous numerical studies and are difficult to observe in laboratory or atmospheric situations. They form a subject in themselves and the details of the flow structures we have found are presented in Mason and Sykes (1979b).

2. Numerical model

The equations of motion are the Navier-Stokes equations for a homogeneous, incompressible, rotating fluid, ie:

$$\frac{\partial \underset{\sim}{u}}{\partial t} + \underset{\sim}{u}.\nabla \underset{\sim}{u} = -\nabla p - \underset{\sim}{f} \wedge \underset{\sim}{u} + \nu \nabla^2 \underset{\sim}{u}$$

$$\nabla . \underset{\sim}{u} = 0$$

where $\underset{\sim}{f} = (0, 0, f)$. Figure 1 defines the coordinate system and geometry, and f is the Coriolis parameter.

The method used for the numerical solution of these equations is a direct extension of the two-dimensional method described in Mason and Sykes (1978d). The variables are stored on the usual staggered mesh, eg Williams (1969). The nonlinear terms are calculated using the energy-conserving form of Piacsek and Williams (1970), and all spatial differences are second-order accurate. The time-derivative is approximated by the leapfrog scheme, hence the viscous terms use the Du Fort Frankel formulation to maintain stability.

The mesh is Cartesian, stretched in all three directions, thus allowing a distribution of grid-points which matches the flow structure. The resulting Poisson equation for pressure is solved on the non-uniform grid by means of a direct reduction method due to Farnell (1979). This method is an extension of the discrete Fourier transform method to a non-uniform mesh, and uses the eigenvectors of the finite difference operator to effect a direct solution. This method is faster and more accurate than the usual ADI technique with the number of grid-points used here. The maximum dimensions of the grid are 40 x 32 x 40 in the (x, y, z)-directions respectively. The direct solution method is used in two dimensions, and the resulting one-dimensional problem is solved by line inversion. The CPU time per timestep with the full mesh is 8s on an IBM 360/195.

The lower non-slip boundary condition on the surface $z = S(x, y)$ is included as described in Mason and Sykes (1978b). The surface passes arbitrarily between the Cartesian grid-points, and the viscous term only is made

accurate at the boundary, by means of special viscosity values around the surface. Other terms in the equations of motion are inaccurate on the surface, but provided the grid-points are sufficiently close to the surface for the viscous term to dominate, there is no real loss of accuracy. Mason and Sykes (1978b) contains a formal estimate of the accuracy of the above method, based on the dynamics of the flow near the surface. In the flows considered in this paper, for which the height of the topography is of the same order as the boundary layer depth, the errors due to the representation of the topography are not the dominant errors. More stringent conditions on resolution arise from the need to close the nonlinear energy cascade to short wavelengths. This places a restriction on the Reynolds

number based on the grid length, but the precise magnitude of the error is

Reynolds number based on the grid length, but the precise magnitude of the error is

difficult to determine due to the uncertainty in the estimates of terms in the equations. From resolution tests in two dimensions, it appeared that values of grid Reynolds number $U_g \Delta / \nu$ of about 20 were adequate (where Δ is the gridlength). We also found that the effects of larger Reynolds numbers (up to about 100) were not too serious, generally only producing grid length scale motions with amplitude up to 20% of the mean amplitude.

In the flows considered here, the rotation plays no real part in the dynamics, apart from providing the basic Ekman boundary layer. The advantage of the Ekman layer is its horizontal homogeneity, allowing the specification of periodic boundary conditions in the x- and y- directions. Although this complicates the details of the local flow, it is necessary if estimates of total momentum transfer due to the presence of topography are required. Theories of laminar flow over small humps, eg. Smith (1973), Smith, Sykes and Brighton (1977) show that the surface stress returns slowly to its upstream value; the decay of the perturbation downstream is algebraic, with a relatively small negative power of distance. In view of this fact, an

extremely large domain of integration would be required to contain all the significant effects of the hill. In a periodic domain, and in the steady state, the entire domain is self-contained, and the total momentum transfer can be ascertained.

The remaining boundary conditions in the vertical direction are

$$\underset{\sim}{u} = 0 \qquad \text{on} \qquad z = S(x,y)$$

$$\frac{\partial u}{\partial z} = \frac{\partial v}{\partial z} = w = 0 \qquad \text{on} \qquad z = D.$$

Results

In all the results presented here we have adopted a standard form of topography. The height of the topography is

$$S = h \cos^2\left[\frac{\pi}{2L}(x^2+y^2)^{\frac{1}{2}}\right] \qquad \text{for } (x^2+y^2) < L^2 \qquad \text{and} \qquad S = 0$$

for $(x^2 + y^2) \geq L^2$. The relative size of the domain varied slightly but was generally $8L$ in the x- direction and $5L$ in the y- direction. This was enough to effectively isolate the topography in all but one case (Run 27; Table 1). The basic non-dimensional parameters determining each integration are a Reynolds numbers, a Rossby number and various ratios of scales. The Rossby numbers $Ro = u_g / Lf$ were always greater than 10 and were typically 100, so effects due to the basic rotation were of no consequence in the dynamics of the flow other than to determine the basic Ekman boundary layer structure. A complete set of consequential parameters was thus $R = h\bar{u}/\nu$, h/δ and h/L where $\bar{u}$ is the mean velocity in the x-direction,

between z=o and z = h, in the undisturbed velocity profile, and $\delta = (2\nu/f)^{1/2}$ is the scale of the Ekman boundary layer. In discussing the results it is convenient in what follows to consider two cases (a) $L/\delta \sim 10$ and (b) $L/\delta \sim 1$

(a) Forces on scales $L \sim 10\delta$

On these scales a significant factor in the integrations is the instability of the basic Ekman boundary layer profile. These instabilities depend on the Reynolds number of the boundary layer $Re = U_g \delta/\nu$ and the first instability to occur is the so-called class A viscous instability (see eg Lilly 1966) at $Re \geqslant 55$. At $Re \geqslant 125$ the class B or inflexion point instability with higher growth rate occurs. The values of Re considered in the present study ranged up to 600 and given a mesh with appropriate resolution, instabilities were triggered. The instability gave rolls with a typical wavelength of 18δ, and an orientation dependent on Re but within $\pm 15^{\circ}$ of the geostrophic wind (in accord with Lilly 1966).

In M & S we discussed such Ekman layer instabilities in a two-dimensional domain aligned with the geostrophic wind and found horizontal diffusion to be a powerful stabilising factor. By rotating the geostrophic wind direction in the two-dimensional model we have been able to investigate some aspects of the stability of rolls which occur in the three-dimensional model without recourse to three-dimensional integrations. When the rolls are not perpendicular to the geostrophic wind, but roughly parallel to it, growth rates are much larger and horizontal diffusion, of reasonable magnitude, is nolonger able to suppress the instabilities. Our interest in suppressing this instability arises from our wish to unambiguously identify the effects of topography. In the next section the boundary layer has been effectively stabilised by restricting the size of the computational domain, and thus the largest possible wavelength, to values smaller than 18δ (typically 5δ). Since computer resources prevent the resolution of processes occuring on widely disparate scales the stabilisation is an almost inevitable consequence of studying scales $\sim \delta$.

Our study of three-dimensional flows involving Ekman rolls is sadly limited. This is a consequence of the long time scale associated with development and

equilibriation of flows involving the rolls. The two-dimensional studies suggest integration times perhaps 10 times as long as those necessary for flow over topography in a similar domain (ie 100 $L/\bar{U}$ cf $10L/\bar{U}$). The main integration (Run 19) involving freely-occurring Ekman rolls had parameters Re = 600 (R = 300), h/δ = 1 and $h/L = \frac{1}{8}$, and a computational mesh of 40 x 32 x 32 points was used. Figure 2 illustrates the vertical velocity field at z = 870 m after $3.3.10^4$ s (=$L/\bar{U}$ x 33) from the start of the integration. The fields are far from steady; the amplitude of the rolls reached a maximum of $w \simeq 0.4$ ms^{-1} at $t = 1.5.10^4$ s, a mimimum of $w \simeq 0.2$ ms^{-1} at $t = 3.0 \times 10^4$ s and are currently increasing in strength. A time-average of the surface stress between the maxima and minima shows a 14% increase im surface stress (confirmed by longer two-dimensional integrations). The pressure force on the topography is very small compared with this change in net viscous stress (comparable to that in Run 30 Table 1) and if the topography is having any significant effect on the net force it must be through the Ekman rolls. It is of interest that the topography clearly affects the phase of the roll disturbances appearing to keep them nearly stationary on a length scale $\sim 3L$ in its lee. Elsewhere in the domain the rolls appear to drift in accord with Lilly's (1966) results from linearised stability theory. To try to quantify this qualitative impression we have averaged the velocity fields over a period of 2.4×10^4 s. During this period the rolls remote from the obstacle drift and at least 5 wavelengths pass over such points of the terrain. Figure 3 shows the mean vertical velocity field at z = 870 m. It follows from the instantaneous amplitudes of the rolls and simple statistics that any value over 0.02 ms^{-1} should represent a significant mean. The main effect occurs in the lee of the obstacle but the whole domain is affected. The amplitude in the lee is about 0.05 ms^{-1} showing that even where the rolls were fairly

stationary some "wobbling" must have occurred. The mean vertical roll structure 1.37×10^4 m downstream of the top of obstacle is illustrated by the vector plot given in Figure 4. The vertical scale of the rolls is seen to be somewhat greater than the depth of the boundary layer and comparable to the horizontal scale of the rolls. To see what effect the topography was having on the net forces it was removed at $t = 1.4 \times 10^4$ s and the integration again continued until $t = 3.3 \times 10^4$ s but with flat terrain. The subsequent behaviour of the net stress, apart from a short term transient, was almost identical to the case with topography. The phase behaviour was however different with the rolls gradually assuming a nearly uniform propagation over the whole domain.

In M & S, topography appeared to excite Ekman rolls in otherwise stable two-dimensional flows. Here, with expensive three-dimensional integrations, we felt we could only justify a single test. Three methods appear open to us to achieve a stable boundary layer (for arbitrary length disturbances), we may either make the Reynolds number Re < 55, employ sufficient horizontal diffusion to make the horizontal Reynolds numbers of the rolls of order unity, or impose a small vertical stratification (Kaylor and Faller 1972). The latter choice undoubtedly has the greatest atmospheric significance and fortunately the value of stratification required is not large enough to significantly affect the dynamics of the flow over the topography. Studies with the two-dimensional model with Re = 600 showed stabilisation to occur with the

Brunt-Vaisala frequency $N = \left[-g/\bar{\rho}\ \frac{\partial \rho}{\partial z}\right]^{1/2}$ greater than a critical value between 2.10^{-3} and $3.10^{-3} s^{-1}$ (g is the acceleration due to gravity, $\bar{\rho}$ the mean density and $\partial\rho/\partial z$ the vertical density gradient in our incompressible fluid). The parameters in the three-dimensional integration were identical to that for run 19 (see above) except that $N = 3.10^{-3} s^{-1}$, giving a $F_L = \frac{2\pi U_0}{NL} = 3$, was used. Since F_L is greater than unity very little gravity wave energy can be produced. In the results no discernable rolls were excited and the forces in this integration (run 30) are discussed in the next section.

(b) Forces on scales $L \sim \delta$

Flows on this scale which produce significant changes in net force involve flow separation. As we mentioned in the introduction, a detailed description of these flows is beyond the scope of this paper and is to be found in Mason and Sykes (1979b). For the purpose of this paper we simply wish to roughly classify these separated flows. Figures 5 to 7 illustrate limiting ($z \longrightarrow S(x,y)$) surface flow trajectories obtained from the surface stress directions. These are a powerful diagnostic in characterising the flow. Figure 5 is typical of separation close to the critical Reynolds number (for a given slope) at which separation first occurs. The separation is confined to the lee of the obstacle. At higher Reynolds numbers and/or slopes, upstream separation such as that illustrated in Figure 6 may also occur. In these flows with upstream separation the well-known horse-shoe vortex formation is found (see eg. Sedney 1973). The horizontal vortex lines of the undisturbed boundary layer are advected towards and trapped at the upstream stagnation point where the flow impinges on the surface. The rest of the vortex line is advected round the obstacle and downstream with concomitant vortex stretching. In the case of Figure 6 the Reynolds number is

so small that the resultant vortex travelling downstream is dissipated on the length scale of the topography. In Figure 7 we show the pattern from a higher Reynolds number flow; strictly (see § 2) this Reynolds number is beyond our computational capabilities and the presence of grid-length features in some fields must be acknowledged. This flow is not steady and the generation of significant trailing vortices (to $\sim 3L$ here) seems to occur at similar parameters to unsteadiness. The swirls evident in the surface stress pattern on the lee side of the obstacle are not related to the horse-shoe vortices but are a feature of lee separation at high Reynolds number (Hunt et al 1978, Sedney 1973).

As we mentioned earlier we adopt a periodic domain to facilitate estimates of net changes in momentum transfer. One penalty which the periodic domain incurs is flow equilibriation on the time scale $B/\bar{U}$ where B is the length of the domain. Thus to make useful estimates of total forces each integration was run for a time scale of about 10 $L/\bar{U}$ i.e. $2B/\bar{U}$ (typically 1200 time steps). We have determined the pressure force on the topography, $\underset{\sim}{P} = (P_X, P_Y)$, and the net viscous force on the surface, $\underset{\sim}{V} = (V_X, V_Y)$, by plotting graphs of these quantities against time. From the graphs we have judged by eye a final value (for unsteady flows a time average) and an estimate of maximum possible error. The errors in $\underset{\sim}{P}$ and $\underset{\sim}{V}$ were generally small but the relative errors in the net change in momentum transfer $\underset{\sim}{T} = \underset{\sim}{V} + \underset{\sim}{P} - \underset{\sim}{V_0}$ (where $\underset{\sim}{V_0}$ is the viscous force on the domain in the absence of topography) were clearly very large when $\underset{\sim}{V}+\underset{\sim}{P}$ was nearly equal to $\underset{\sim}{V_0}$.

In Table 1 we summarise the basic parameters, flow characteristics and net forces for the integration we present here.

In Figure 8 we consider obstacles with $h = L = \delta$, i.e. slope of unity and height equal to the boundary layer scale, and vary the Reynolds number.

Two of the quantities plotted are the x-direction pressure drag coefficient $C_{PX} = P_x / \frac{1}{2}\bar{\rho}A\bar{U}^2$ (where A is the frontal area of the obstacle) and an efficiency factor $E_{PX} = T_x / P_x$ representing the net change in x-direction momentum transfer. For large Reynolds number, C_{PX} would on general grounds (Batchelor 1967 p.339) be expected to be ~ 1. At R = 300 this is true and the efficiency factor is also ~ 1. This situation accords with the general rules upon which net momentum transfer estimates in the atmosphere have been made (see eg Smith 1975). At $R = 100$ both C_{PX} and E_{PX} have been reduced so that $C_{TX} = T_x / \frac{1}{2}\bar{\rho}A\bar{U}^2$ (see Table 1) is nearly a factor of 3 or less. At R = 30, C_{PX} has risen, this is probably due to the increased viscous stress of the lower Reynolds number flow and is more in evidence at R = 10 when C_{PX} is comparable with estimates for low Reynolds number flow. However, at both R = 30 and 10 the efficiency E_{PX} is essentially zero; the calculations are not accurate enough to give the sign of T_X reliably although we presume negative values to be unlikely and unsupported by analysis. It thus appears that for topography with slopes of unity, Reynolds numbers $R \geq 100$ are required for significant net x-direction momentum transfer. At smaller Reynolds numbers the x-direction pressure force is nearly balanced by a reduction in x-direction viscous stress. The forces in the transverse direction show a different behaviour. The y-direction pressure force is indicated in Figure 8 by the ratio P_Y/P_X. This ratio does not vary significantly with R and the nearly constant value of about 0.6 is consistent with the smaller values of y-direction flow in the basic Ekman boundary layer. Values of C_{TY} are given in Table 1; unlike C_{TX}, which tended to zero as R became small, C_{TY} increases. This is not due to changes in the pressure force but due to the viscous stress V_Y remaining near to its undisturbed value. Since this behaviour does not occur in the small R examples (discussed below) with $h/\delta < 1$ it seems to be a feature of flow with $h/\delta \sim 1$.

In Figure 9 we explore how the forces depend on the horizontal length scale L with $h = \delta$ and R = 100 (except for the data at $L/\delta = 8$ for which R = 300). The prime variable is thus the topographic slope. The data for $L/\delta = 1$ is the same data at that at R = 100 on Figure 8. For smaller L the separation is more violent and both Cp_x and Ep_x are increased, although in the limit of small L/δ and consequent low Reynolds number flow about a thin vertical cylinder, we would not expect this trend to continue. For larger L we see that both C_{px} and E_{px} steadily decrease even though the flow remains separated. It is not clear whether the apparently more rapid fall between $L/\delta = 3$ and 8 is significant, although the higher Reynolds number of the latter flow may have actually increased its relative effect. In either case the net changes in momentum transfer are clearly small for slopes of less than 1 in 3. In many applications it is appropria to compare the net change in momentum transfer with the viscous force $\underset{\sim}{V}_H = (V_{Hx}, V_{HY}$ acting on a flat surface with area equal to the base of the topography. It is clear that since $|\underset{\sim}{V}_H|$ is proportional to L^2 whilst the scale $\frac{1}{2}\bar{\rho} A \bar{U}^2$ is proportional to L, the relative effect of shallow topography is even less than that implied by Figure 9. Values of $E_{Vx} = T_x / V_{Hx}$ are given in Table 1. The y-direction forces do not show any marked variations but some tendencies can be discussed. In particular for larger values of L, P_y/P_x (Figure 9) is reduced a little and as can be seen in Table 1 C_{Tx}/C_{Ty} increases a little. No explanation occurs to us but since upstream separation does not occur with large L this behaviour may be related to changes in flow type.

In Figure 10 we illustrate the effect of varying h with $L = \delta$ and Re = 200. This study was made with a view to investigating the dependence of flow pattern on h/δ and in the present context must be examined carefully. As h reduces so does the Reynolds number R (see Table 1) and the effects on the forces are primarily a consequence of the Reynolds number dependence. The results for $h/\delta = 1$ are also given in Figures 8 and 9. For $h/\delta < 1$, Ep_x is seen to rapidly tend to zero whilst, as at low R in Figure 8, Cp_x increases, These results indicate that the relative scale of the boundary layer, h/δ, is not a dominant factor in determining the x-direction forces.

The y-direction forces do show some systematic variation with h/δ ; as h/δ becomes small the obstacle is exposed to a basic flow at 45° to the x and y directions with a consequent tendency to symmetry. This is reflected in both P_Y/P_X and C_{TY}/C_{TX} tending to unity as h/δ tends to zero.

Conclusions

We have made a range of numerical integrations of three-dimensional laminar flow over surface-mounted obstacles. These flows have ranged from fully attached viscous flow to violent separation. In each case the pressure force on the obstacle had a magnitude in keeping with simple ideas. However, the net change in x-direction momentun transfer which the obstacle produced was only as big as this pressure force for flows with violent separation (involving upstream separation). At smaller slopes and for Reynolds numbers when only downstream separation or fully attached flow occurred, the x-direction pressure force was nearly balanced by a reduction in x-direction surface stress. As with the similar result obtained for two-dimensional flows in Mason and Sykes (1979a) this small net force is in keeping with predictions of both 'triple deck' and low Reynolds number theory. It appears that the occurrence of a significant change in net x-direction force requires eddy motions which transport momentum to the surface. In two dimensions this can only occur when eddies (transverse to basic flow) are shed by the topography. With steady separation the only transfer across the separating streamline is viscous diffusion. In three-dimensional flows such eddy motions are possible with longitudinal rolls and can occur in steady flows. The present work suggests that the principal source of the longitudinal rolls may be the horseshoe vortex mechanism.

In Mason and Sykes (1979a) two-dimensional topography appeared able to excite disturbances similar to Ekman rolls. The boundary layer used in that study was unstable to disturbances at angles close to the geostrophic wind. In the present three-dimensional study the only effect of obstacles

on these freely occurring Ekman rolls was to hold them nearly stationary in their lee. This may be related to the atmospheric observations of stationary rainbands in the lee of topography (Browning and Bryant 1975), and also to the stationary rolls downstream of a heat island (Kropfli and Kohn , 1978). A single test with a stable boundary layer flow did not show three-dimensional topography to excite any rolls.

References

Batchelor, G K 1967 "An Introduction to Fluid Dynamics" Cambridge University Press.

Browning, K A & Bryant, G W 1975 "An example of rainbands associated with stationary longitudinal circulations in the planetary boundary layer" QJ Roy. Met. Soc. 101 pp 893-900.

Farnell, L 1979 "Solution of Poisson equations on a non-uniform grid" Submitted to J. Comp. Phys.

Hunt, J C R; Abell, C J; Peterka, J A & Woo, H 1978 "Kinematical studies of the flows around free or surface mounted obstacles; applying topology to flow visualisation" J. Fluid Mech. 86 pp 179-200.

Kaylor, R E & Faller, A J 1972 "Instability of the stratified Ekman boundary layer and the generation of internal waves" J. Atmos. Sci. 29 pp 497-509.

Lilly, D K 1966 "On the instability of Ekman boundary flow" J. Atmos. Sci. 23 pp 481-494.

Mason, P J & Sykes, R I 1978a "On the interaction of topography and Ekman boundary layer pumping in a stratified atmosphere" QJ Roy. Met. Soc. 104 pp 475-470.

1978b "A simple Cartesian model of boundary layer flow over topography" J. Comp. Phys. 28 pp 198-210.

1979a "Separation effects in Ekman layer flow over ridges" To appear in QJ Roy. Met. Soc..

1979b "Three-dimensional numerical integrations of the Navier-Stokes equations for flow over surface-mounted obstacles" To appear in J. Fluid Mech.

Kropfli, R A & Kohn, N M 1978 "Persistent horizontal rolls in the urba mixed layer as revealed by dual-Doppler radar" J. Appl. Met. 17 pp 669-676.

Piacsek, S A & Williams, G P 1970 "Conservation properties of convection difference schemes"
J. Comp. Phys. 6 pp 392-405

Sedney, R 1973 "A survey of the effects of small protuberances on boundary-layer flows"
A.I.A.A. Journal 11 pp782-792

Smith, F B 1975 "Turbulence in the atmospheric boundary layer"
Sci. Prog. Oxf. 62 pp127-151

Smith, F T 1973 "Laminar flow over a small hump on a flat plate"
J. Fluid Mech. 57 pp803-824

Smith, F T; Sykes, R I; & Brighton, P W M 1977 "A two-dimensional boundary layer encountering a three-dimensional hump"
J. Fluid Mech. 83 pp163-176

Sykes, R I 1978 "Stratification effects in boundary layer flow over hills"
Proc.Roy.Soc.Lond.A 361, pp 225-243

1979 Ph.D Thesis, University of London.
(To be submitted)

Williams, G P 1969 "Numerical integration of the three-dimensional Navier-Stokes equations for incompressible flow"
J. Fluid Mech. 37 pp727-750

Wang, C.-Y. 1978 "Drag due to a striated boundary in slow Couette flow"
Phys.Fluids 21, pp.697-698.

Legends

Figure 1 Schematic geometry of the domain of integration.

Figure 2 Horizontal section through the vertical velocity field at z = 870m. The contour interval is 0.06 ms^{-1}, and solid contours denote positive values. Grid-point positions are indicated by tick-marks on the boundary.

Figure 3 Horizontal section through the time-averaged (see text) vertical velocity field at z = 870m. The contour interval is 0.05 ms^{-1} and solid contours denote positive values.

Figure 4 Vertical section through the time-averaged (see text) velocity vector field in the y-z plane 1.37×10^4 m downstream of the top of the obstacle. The mean flow at each level has been removed to illustrate the roll motion.

Figure 5 Surface stress directions with R = 30. The dashed circle indicates the base of the hill.

Figure 6 As figure 5, but R = 100.

Figure 7 As figure 5, but R = 300.

Figure 8 Graph of pressure drag coefficient, C_{pX}, 'efficiency factor', E_{pX}, and ratio of y-direction force to x-direction pressure force P_Y/P_X against Reynolds number, R.

Figure 9 Graph of C_{pX} and E_{pX} and P_Y/P against non-dimensional base width, L/δ

Figure 10 Graph of C_{pX} and E_{pX} and P_Y/P against non-dimensional height, h/δ

Table 1(a)

Basic parameters used in the numerical integrations

and main features of the resulting flow

Run Number	h/δ	h/L	R	Upstream Separation Occurs	Downstream Separation Occurs	Flow Steady
21	1	1	316	YES	YES	NO
22	1	1	100	YES	YES	YES
23	1	1	30	NO	YES	YES
24	1	1	10	NO	NO	YES
25	1	3	100	YES	YES	YES
26	1	$\frac{1}{3}$	100	NO	YES	YES
27	2	2	300	YES	YES	NO
28	$\frac{1}{2}$	$\frac{1}{2}$	24	NO	YES	YES
29	$\frac{1}{4}$	$\frac{1}{4}$	6	NO	NO	YES
30	1	$\frac{1}{8}$	300	NO	YES	YES

Table 1(b)

Net forces from integrations

Run Number	$C_{Tx} = \frac{\overline{T_x}}{\frac{1}{2}\bar{\rho} A \bar{u}^2}$	$E_{Vx} = \frac{\overline{T_x}}{\overline{V}_{Hx}}$	$C = \frac{T_Y}{\frac{1}{2}\rho A \bar{u}^2}$
21	0.80 ± 0.12	63 ± 10	0.35 ± 0.05
22	0.32 ± 0.08	25 ± 5	0.20 ± 0.04
23	0.04 ± 0.20	2 ± 14	0.30 ± 0.1
24	-0.15 ± 0.20	-10 ± 14	1.00 ± 0.1
25	0.55 ± 0.10	132 ± 22	0.31 ± 0.08
26	0.24 ± 0.10	7 ± 2	0.21 ± 0.05
27	0.70 ± 0.20	180 ± 48	0.25 ± 0.12
28	0.28 ± 0.20	6 ± 4	0.21 ± 0.07
29	0.00 ± 0.60	0 ± 3	0.00 ± 0.30
30	0.03 ± 0.01	0.3 ± 0.08	0.03 ± 0.01

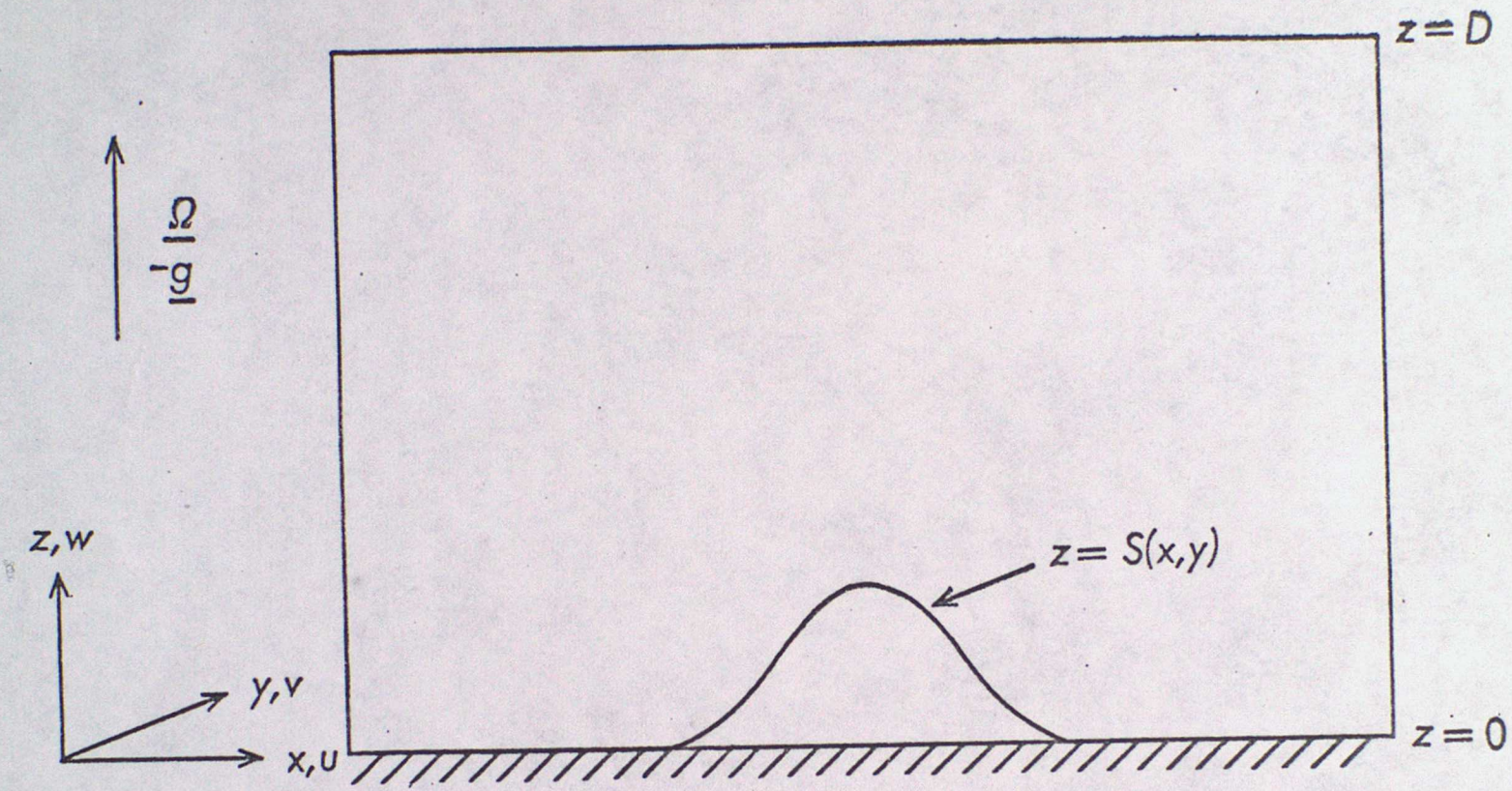

Fig. 1

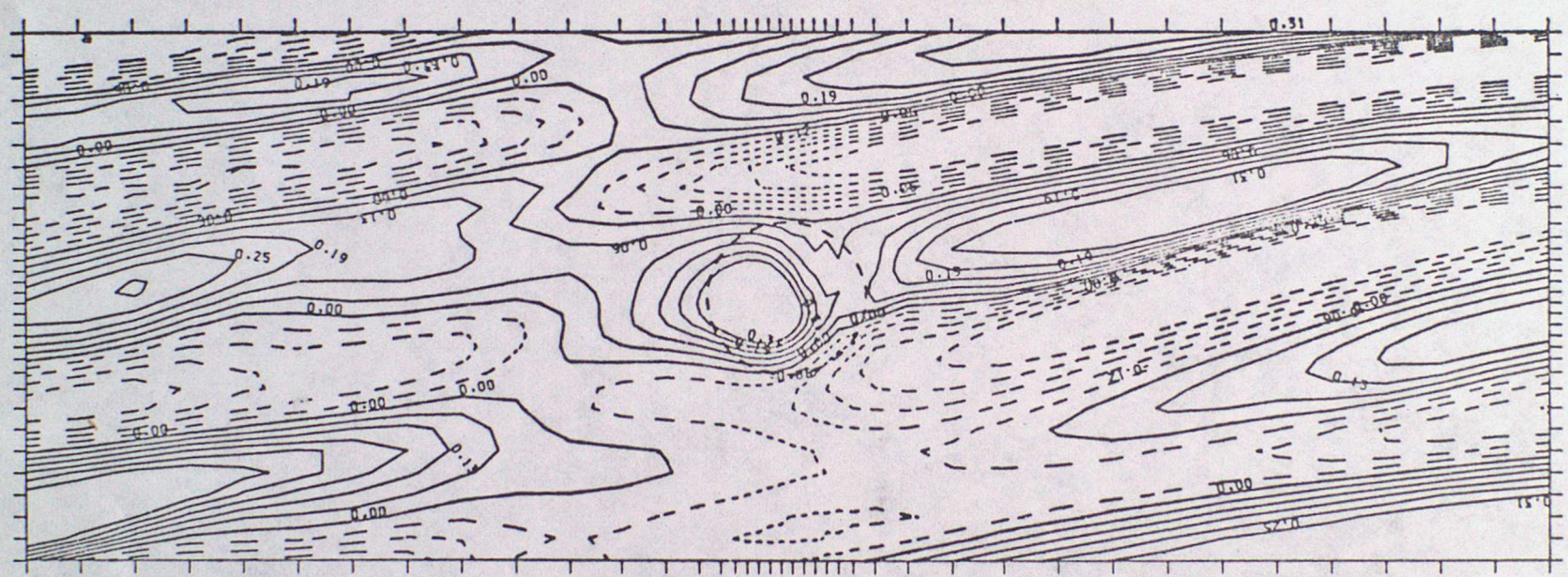

Fig 2

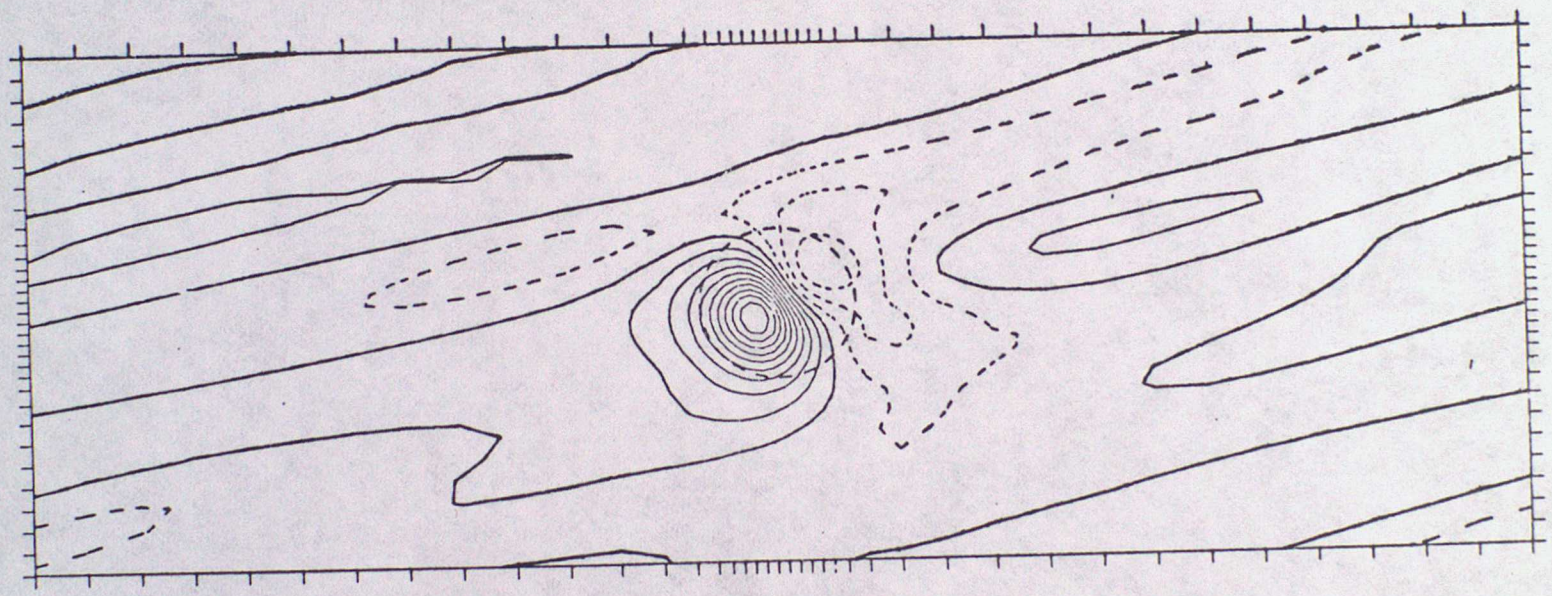

Fig. 3

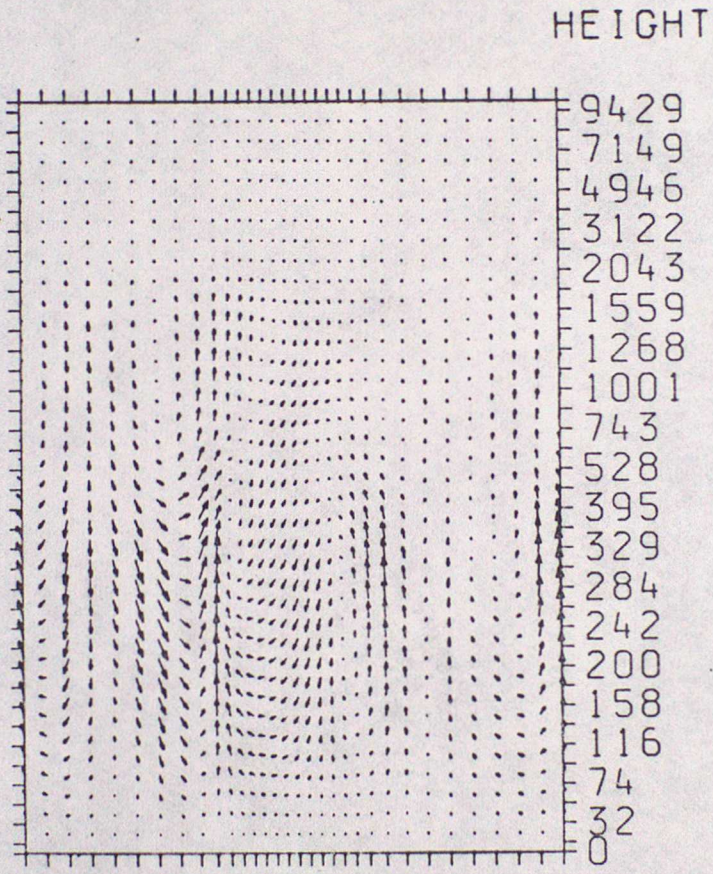
HEIGHTS
9429
7149
4946
3122
2043
1559
1268
1001
743
528
395
329
284
242
200
158
116
74
32
0

Fig. 4

Fig 5

Fig. 4

Fig. 7

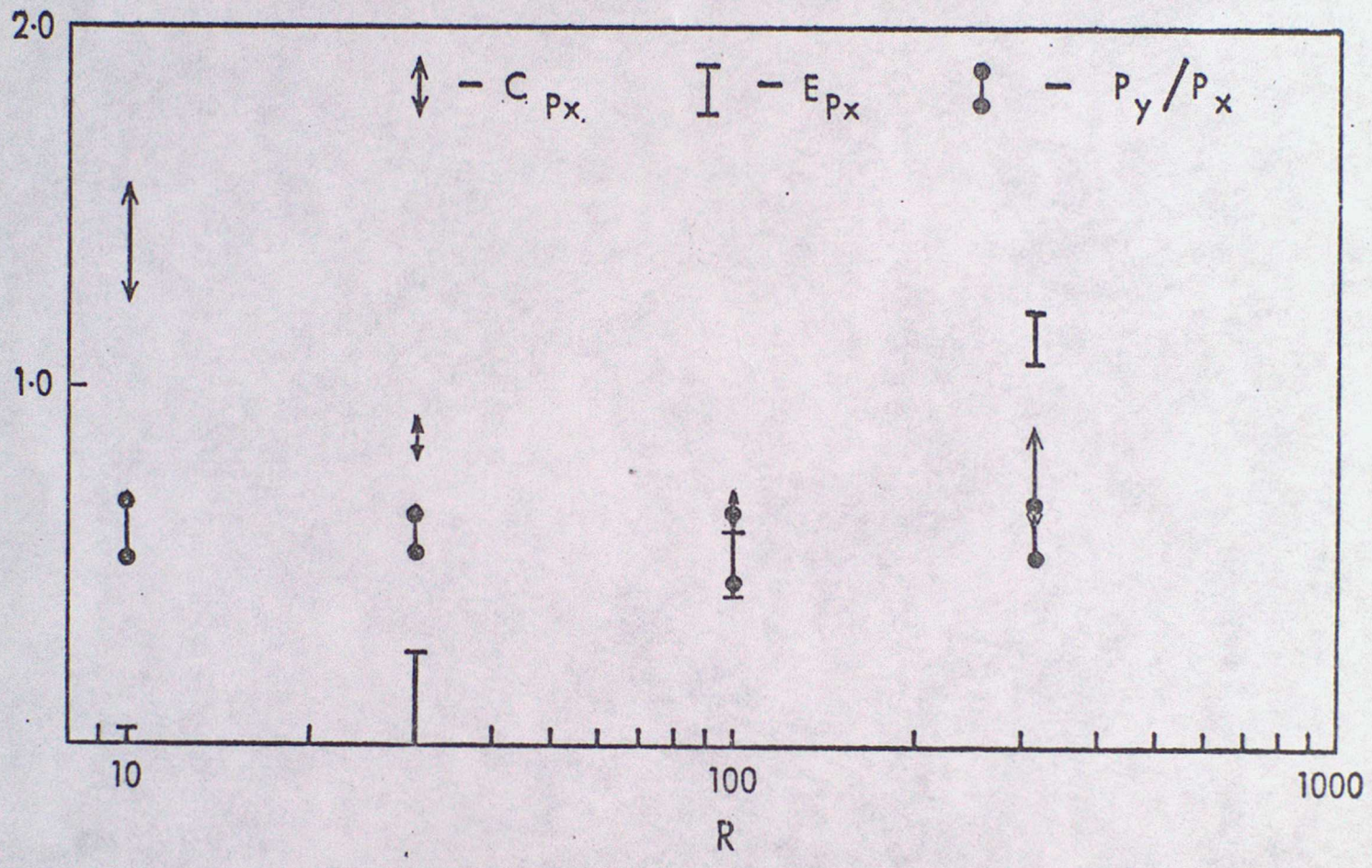

Fig. 8

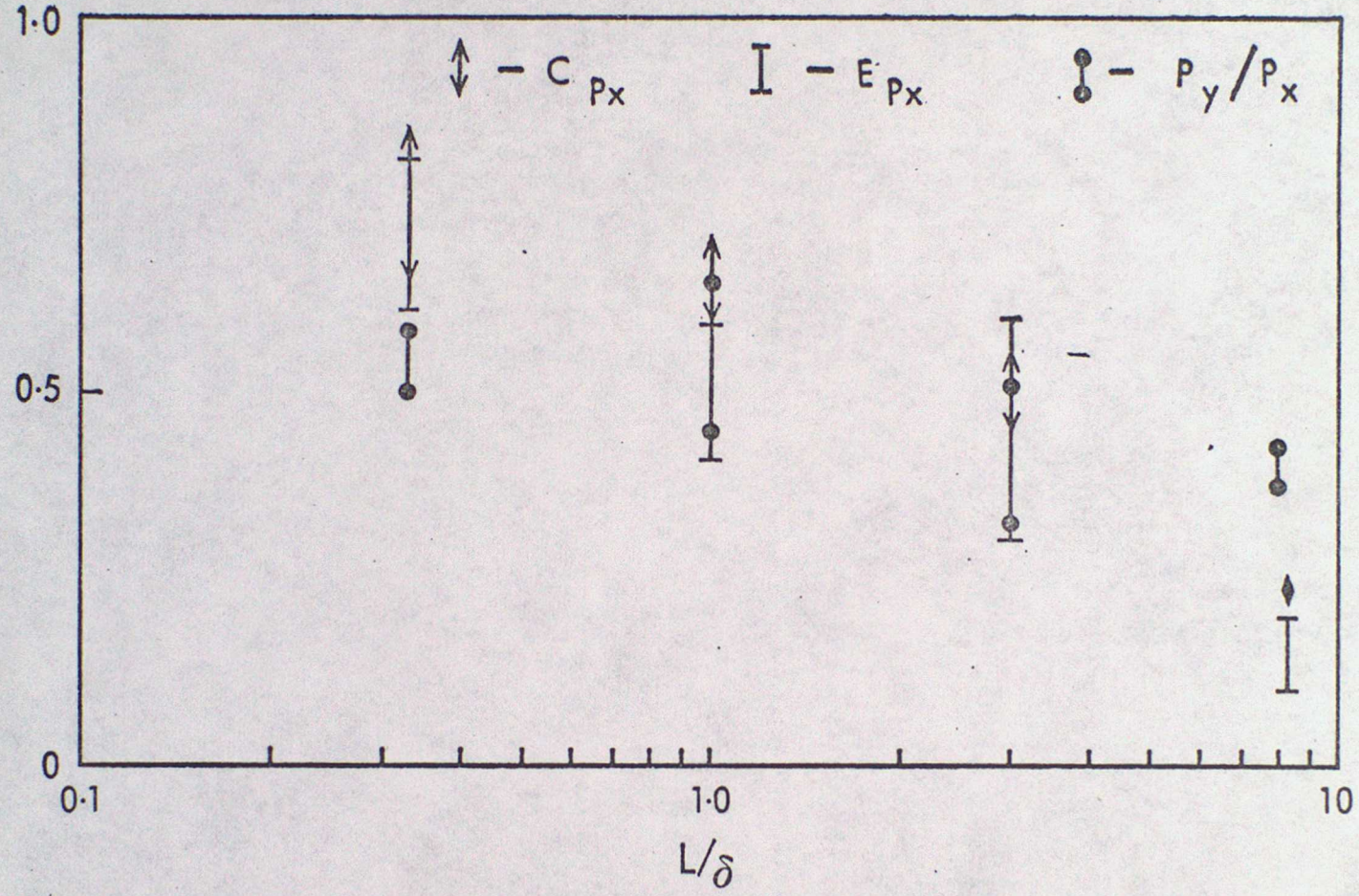

Fig. 9

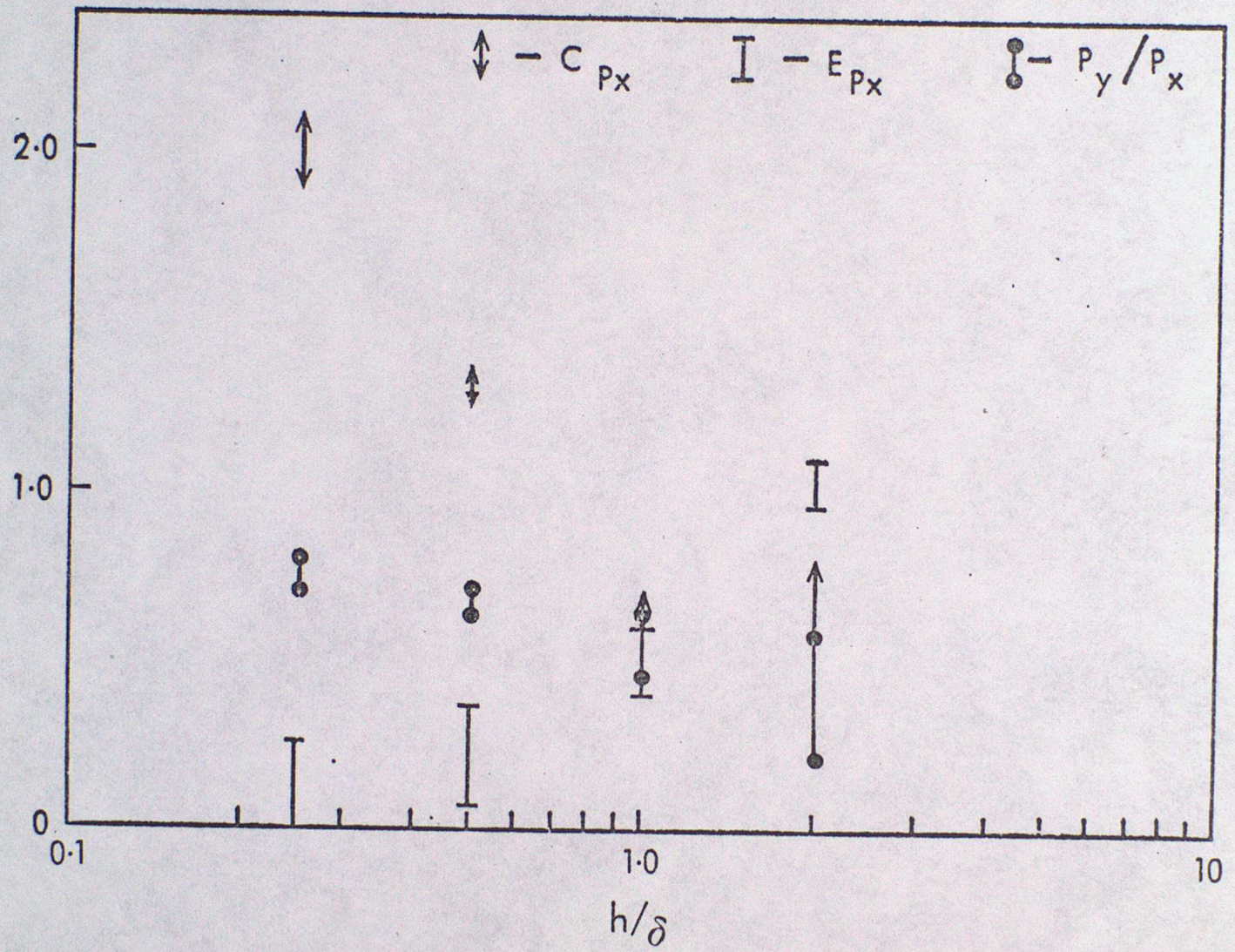

Fig. 10